



# Photocatalytic performance of porous TiO<sub>2</sub> layers prepared by quantitative electrophoretic deposition from organic solvents

Radek Zouzelka, Monika Remzova, Libor Brabec, Jiri Rathousky\*

J. Heyrovsky Institute of Physical Chemistry of the CAS, v.v.i., Dolejskova 3, Prague 18223, Czech Republic



## ARTICLE INFO

**Keywords:**  
EPD  
Photocatalysis  
TiO<sub>2</sub>  
4-chlorophenol  
Water purification

## ABSTRACT

Highly-crystalline TiO<sub>2</sub> nanoparticles coated on a suitable substrate make excellent photocatalysts for environmental applications. While electrophoretic deposition is frequently used to prepare such layers on a conductive support, this method often requires the presence of an additive to suppress nanoparticle agglomeration and increase particle surface charge. However, the presence of an additive can lead to contamination that negatively affects layer properties. To overcome this drawback, we developed an optimized electrophoretic method for the preparation of porous TiO<sub>2</sub> layers, whose photocatalytic performance in the degradation of a toxic compound was analyzed. Our method enabled TiO<sub>2</sub> layers (anatase, rutile and their mixture) to be quantitatively deposited on rigid substrates (stainless steel, FTO-glass and silicon wafers) without sintering and without the use of a dispersive additive. The photocatalytic performance of layers depended on the structural properties of titania particles, especially their allotropic form (anatase vs. rutile) and crystallinity, and on the presents of defects within the crystals. For well-developed crystals of anatase phase a high rate of the degradation of 4-chlorophenol and its almost complete mineralization were achieved. Owing to their excellent properties, especially stability and photocatalytic performance, the layers prepared by EPD are suitable for a broad range of environmental applications.

## 1. Introduction

Electrophoretic deposition (EPD) is a promising method for preparing titanium dioxide layers for use in the photocatalytic degradation of organic water pollutants [1–3]. Such photocatalysts have been mostly tested in powder form, which is favorable in terms of the mass transport of reactants and degradation products [4–6]. However, to avoid the complicated separation or filtration steps of very fine particles, immobilized photocatalysts are increasingly preferred [7–11]. Owing to the formation of thin layers on the surface of technically important materials, such as stainless steel and glass, these materials acquire a new functionality, which is important for the protection of their surface and for the remediation of the environment.

To achieve a successful deposition, both suspension and process parameters need to be optimized. Suspension parameters include the particle size, particle zeta potential, liquid relative permittivity, along with the suspension conductivity, viscosity and stability [12–15].

Regarding particle size, deposition of various ceramic and clay particles of up to 20 µm in size was reported [16]. The fact that particle mobility under electrophoresis must be higher than that under gravity determines the upper particle size limit. Particle size seems to have a

pronounced effect on the cracking of deposits during drying; for example, for particles less than about 100 nm, cracking was found to be substantially reduced [17]. The suppression of layer cracking during drying is essential if we are to obtain high-performance layers with good enough mechanical properties for use as superconductive films, glass composites or layered ceramics, all of which require annealing at high temperatures.

Together with particle size, the zeta potential of the particles, which is directly proportional to their mobility, is of utmost importance, with an absolute value of at least 30 mV being preferable [12]. Zeta potential plays a decisive role in three areas: (i) stabilizing the suspension through repulsive interaction between the particles, (ii) determining the direction and migration velocity of the particles during deposition, and (iii) influencing the apparent density of the deposited layer [18]. The zeta potential can be controlled by changing the suspension pH or by the specific adsorption of electrolytes, both of which, however, are often undesirable because of the risk of contaminating the deposited material.

In terms of the suspension as a whole, the properties of the continuous liquid phase have a considerable influence on the electro-deposition process. The relative permittivity and liquid conductivity

\* Corresponding author.

E-mail address: [jiri.rathousky@jh-inst.cas.cz](mailto:jiri.rathousky@jh-inst.cas.cz) (J. Rathousky).

should be neither too high nor too low, while suspension viscosity should be preferably low, up to a maximum of several mPa s [19]. When the relative permittivity is lower than about 10, deposition fails because of insufficient dissociative power. Conversely, when the relative permittivity is too high (around 80 or above), the high ionic concentration in the liquid reduces the thickness of the double layer and, consequently, its electrophoretic mobility. If the suspension is too conductive, particle motion is very low, and if the suspension is too resistive, the particles charge electronically and stability is lost [14,15,20].

Turning to the process itself, the most important parameters are deposition time, applied electric field, solids concentration in the suspension and substrate conductivity. While deposition is linear during its initial stage, its rate decreases and finally attains a plateau at very long deposition times. Regarding electric field, more uniform films have been deposited at moderate applied fields ( $25\text{--}100\text{ V cm}^{-1}$ ) while film quality deteriorates if relatively high applied fields ( $>100\text{ V cm}^{-1}$ ) were used [21]. The volume fraction of solids in the suspension also plays an important role, particularly for multi-component EPD. Because a threshold for the concentration of particles in the suspension has been identified [22], this parameter too must be carefully considered. Below this threshold, no deposit growth occurs independently of the applied electric field and deposition time. For instance, the threshold concentration for titania particles at  $250\text{ V cm}^{-1}$  is around 0.1 vol.% [23]. For successful electrophoretic deposition of nanoparticles the substrate must be conductive [18]. Otherwise, the electrical circuit is not closed and consequently the migration of charged particles to the electrode is stopped.

Finally, a very important parameter is the percentage of particles, which is really deposited. The complete deposition is an optimum as often-valuable material is effectively used without any losses and the necessity to determine the mass of the deposited particles is removed. Further, the deposition time is not necessary to be determined beforehand as the deposition can be simply finished after the clarification of the dispersion. However, to the best of our knowledge these features of EPD have not been addressed in the literature yet.

In this study, we optimized the suspension and process parameters of the EPD process to prepare highly-crystalline porous  $\text{TiO}_2$  layers for pollutant degradation. Our aim was to achieve a quantitative deposition of main structural forms of  $\text{TiO}_2$  important regarding their photocatalytic application (i.e., anatase with vastly different particle size, rutile, a mixture of anatase and rutile) on stainless steel, silicon and conducting glass plates. Our attention was focused on identifying the optimum continuous phase (various organic solvents including their mixtures), applied electric field and the concentration of dispersed solid particles. To avoid potential contamination of the deposited layer, no additives were used. To enable the potential application of this method also for temperature-sensitive materials (such as conducting polymers and heat-sensitive particles), the whole process was carried out at  $25^\circ\text{C}$ . Our criteria for successful quantitative deposition were the layer homogeneity, good mechanical stability in aqueous media, good adhesion to the substrate, and, in particular, high photocatalytic efficacy

in the 4-chlorophenol degradation. A major attention was also devoted to the explanation of the mechanism of the photocatalytic degradation of 4-chlorophenol and the achievement of almost complete mineralization.

## 2. Materials and methods

### 2.1. Materials and characterization

**Aeroxide<sup>®</sup>**  $\text{TiO}_2$  P25 (Evonik,  $\geq 99.5\%$  on trace metals basis) (hereinafter referred to as P25) is titania photocatalyst widely used owing to its high activity in many photocatalytic reactions. It often serves as a standard, containing more than 70% of anatase phase with a minor proportion of rutile (about 20%) and a small percentage of amorphous phase [24]. It exhibits a specific surface area in the range of  $35\text{--}65\text{ m}^2\text{ g}^{-1}$  (according to the manufacturer). To purify it mainly from hydrochloric acid, P25 was thoroughly washed with deionized water followed by centrifugation. In particular, 48 g of the P25 powder was added to 900 mL of deionized water, stirred overnight and then ultracentrifuged in a Beckman Coulter Optima<sup>™</sup> XPN apparatus at 208 000g for 30 min at  $25^\circ\text{C}$ . This process was repeated six times. The presence of chloride ions and the conductivity of the supernatant were measured potentiometrically using a WTW inoLab pH 7310.

Anatase (BDH Chemical Ltd., at least 99%) (hereinafter referred to as Anatase) exhibits high phase purity. Hombikat UV 100 (Sachtleben, approx. 99%) (hereinafter referred to as UV 100) contains also exclusively the anatase phase. Highly pure rutile nanopowder (Merck, 99.5% trace metals basis, designated as Rutile) exhibits the primary particle size of up to 100 nm (according to the manufacturer).

The crystallinity of titania powders was measured using a D5000 high-resolution X-ray diffractometer (Siemens) operated at 40 kV and 45 mA with  $\text{Cu K}\alpha$  radiation ( $\lambda = 1.5406\text{ \AA}$ ). The texture properties of powders and layers were determined by the analysis of adsorption isotherms of nitrogen or krypton at ca 77 K performed with a Micrometrics 3FLEX volumetric adsorption unit. The optical properties of layers were measured with a Lambda 950 UV-vis-NIR spectrometer (Perkin Elmer) equipped with Spectralon and gold integration spheres for diffuse reflectance measurements in the UV-vis-NIR region, and with a Fourier transform infrared spectrophotometer Nicolet 6700. The surface morphology of layers was studied with a scanning electron microscope JSM-6700F (Joel).

### 2.2. Preparation of titania layers by EPD

First, titania particles were dispersed in ethanol (96%), i-propanol or acetone (Table 1). Afterwards, this dispersion was injected into either tetrahydrofuran or acetone. Alternatively, we used a mixture of acetone, tetrahydrofuran and heptane (Table 1). All solvents (p.a. purity) were supplied by Penta (Czech Republic).

In EPD the electric field was adjusted to  $300\text{ V cm}^{-1}$  using DC power supply EV245 (Consort, Belgium). Polished stainless-steel plates, fluorine-doped tin oxide glass sheets (FTO) and very smooth silicon

**Table 1**

The properties of powders and solvents used for the EPD process.

Photocatalyst	$S_{\text{BET}}/\text{m}^2\text{ g}^{-1}$	d/nm	Dispersant	$\zeta/\text{mV}$	Injected into	$\zeta/\text{mV}$	Working electrode
P25	57	26	EtOH	-17	THF	+20	cathode
UV 100	271	5	EtOH	-12	THF	+25	cathode
			i-PrOH	-43	THF	+17	cathode
Anatase	10	150	i-PrOH	-26	Act	-51	anode
			i-PrOH	-26	Act:THF 1:1	-26	anode
Rutile	26	58	Act	-55	Act:Hept 1:1	-26	anode
			Act	-55	Act:Hept 1:2	-30	anode

$S_{\text{BET}}$ , BET surface area; d, particle size calculated from  $S_{\text{BET}}$  provided the crystals were approximated by spheres;  $\zeta$ , zeta potential (Hückel approximation); EtOH, ethanol (96%); i-PrOH, isopropanol; Act, acetone; THF, tetrahydrofuran; Hept, heptane.

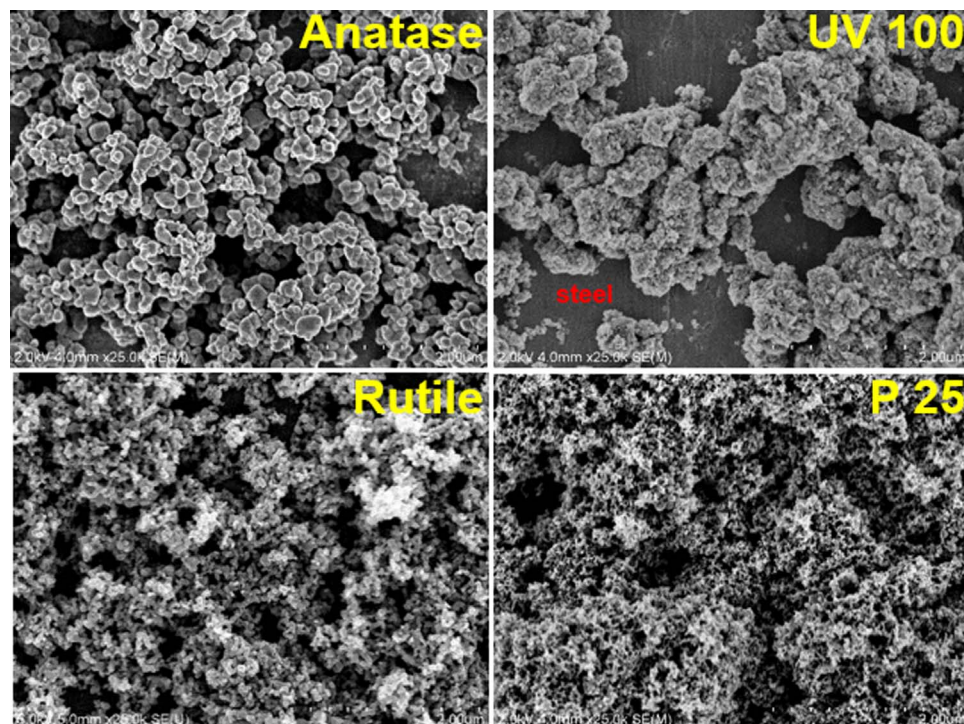


Fig. 1. SEM top-view of  $0.12 \text{ mg cm}^{-2}$  of titania deposited on stainless steel.

wafers naturally oxidized (all of the substrates were  $20 \text{ mm} \times 40 \text{ mm}$  in size) served as the working electrodes (anode or cathode). A stainless-steel plate was used as a counter electrode. The distance between vertically placed electrodes was 11 mm. Prior to EPD, electrodes were washed ultrasonically in deionized water and acetone. The titania loading on the support was between  $0.03$  and  $2.5 \text{ mg cm}^{-2}$ . 10 min of EPD process was found sufficient for the deposition of all dispersed titania particles.

### 2.3. Photocatalytic measurements

An aqueous solution of 4-CP ( $0.1 \text{ mmol L}^{-1}$ ) was photocatalytically degraded at  $25^\circ\text{C}$  on titania layers ( $4.0 \text{ cm}^2$ ) in a  $25 \text{ mL}$  quartz cell. As the top of the liquid in the cell was open to air and the solution was intensively stirred, the concentration of dissolved oxygen was constant during the experiment. A Sylvania Lynx-S 11 W BLB lamp irradiated the layer surface with UV light ( $365 \text{ nm}$ ) at a low power density of  $1.0 \text{ mW cm}^{-2}$ . Prior to the photocatalytic experiments, the dissolved 4-chlorophenol was equilibrated with the photocatalyst surface for three hours. For each experiment, eight small aliquots each of  $100 \mu\text{L}$  were taken from the solution in the reaction cell at regular time intervals and analyzed by high-performance liquid chromatography [25]. The first-order rate constants for the 4-chlorophenol degradation were calculated using a nonlinear regression fitting of the kinetic curves. Supplementary photocatalytic experiments were conducted to distinguishing between the reaction pathways based of the radical mechanism or on the direct charge transfer from the photocatalyst to the 4-chlorophenol molecule. In these experiments, an excess of 2-propanol ( $10^{-1} \text{ M}$ ) was added to the reaction mixture while irradiation was continued to scavenge the formed radicals. To evaluate the degree of mineralization of 4-CP molecules at the end of the experiment, the total organic carbon concentration (TOC) was determined using a TOC-L Analyser (Shimadzu).

## 3. Results and discussion

### 3.1. Optimization of the EPD technique

In order to quantitatively prepare easily reproducibly  $\text{TiO}_2$

photocatalytic layers of desired mass without using additives (e.g. binders, surfactants), EPD should be carried out under highly specific conditions. Using novel mixtures of organic solvents and strong electric field, we found that quantitative deposition was feasible. Furthermore, the layers prepared were ready for photocatalytic testing immediately after EPD and fast volatile solvent evaporation. Neither heating for drying nor calcination for layer consolidation was necessary because the deposited titania did not contain additional impurities and was sufficiently mechanically stable when immersed in aqueous media.

The optimized EPD process developed in this study enabled the preparation of  $\text{TiO}_2$  layers of a mass up to  $2.5 \text{ mg cm}^{-2}$ . Using our method, all of the particles dispersed in an organic solvent were completely deposited on the substrates used. Stainless steel sheets and FTO glasses were selected as conductive supports. Silicon plates, with a thin surface film of  $\text{SiO}_2$  ( $\sim 5 \text{ nm}$ ) on their surface, were also suitable because the electrical resistance of the organic suspensions predominated. None of the used supports affected the quality of the deposited layers.

We identified the most suitable solvents (acetone, heptane, tetrahydrofuran, ethanol and 2-propanol) for  $\text{TiO}_2$  powder deposition without the use of additives. These solvents were selected with respect to their low toxicity, sufficient volatility and suitable electric properties (especially relative permittivity and conductivity).

Depending on the solvent used, the  $\zeta$ -potentials of the  $\text{TiO}_2$  particles were either positive or negative (Table 1). The dispersed particles were stable in the dispersion and the solvent determined the direction of their electrophoretic migration. The settling of particles was negligible due to their low concentration ( $< 0.5 \text{ g L}^{-1}$ ) and small particle size (Table 1).

### 3.2. Optimized deposition methods

To obtain high quality layers, suitable organic solvents should be judiciously combined. According to the solvents used and the properties of particles, they migrated either to cathode or anode working electrode. The selected solvents enabled to apply a high intensity of the electric field ( $300 \text{ V cm}^{-1}$ ). The experimental conditions neither influenced the physico-chemical properties of deposited particles nor were detrimental to the layer stability. As, however, none of the solvent

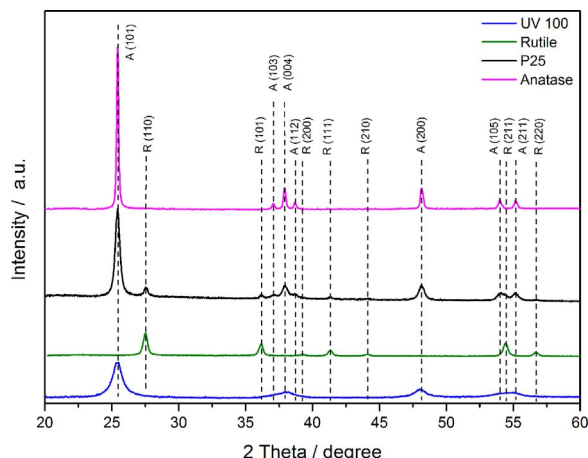


**Fig. 2.** XRD patterns of the investigated UV 100 (blue), Anatase (magenta), Rutile (olive) and P25 (black) titania layers. (For interpretation of the references to colour in this figure legend, the reader is referred to the web version of this article).

combinations was universal, we had to find the optimum for each type of particles (**Table 1**).

### 3.3. Morphological and structural properties of porous titania layers

Scanning electron microscopy (SEM) observation showed a significant difference in the surface morphology of the deposited layers of different titania powders (**Fig. 1**). In **Table 1** the BET surface area and average particle size of all the used powders are summarized.

UV 100 powder consisted of large agglomerates roughly 0.5–1 µm in size of small primary particles of only about 5 nm. These agglomerates were highly porous as confirmed by nitrogen adsorption experiments, which provided a very large surface area of 271 m<sup>2</sup> g<sup>-1</sup>. If 0.12 mg cm<sup>-2</sup> of UV 100 were deposited on steel, the agglomerates formed a highly irregular coverage with substantial parts of the support uncovered (**Fig. 1**). The other three materials (Anatase, Rutile, P25) were less agglomerated and completely covered the steel surface at the same loading as UV 100 (**Fig. 1**).

The structural properties of the prepared layers were investigated by X-ray diffraction (**Fig. 2**). The diffraction pattern of P25 exhibited reflections both of anatase and rutile phases, indexed at (101) 25.40°, (103) 36.98°, (004) 37.90°, (112) 38.63°, (200) 48.16°, (105) 53.95°, and (211) 55.16°, corresponding to a tetragonal anatase structure (space group I4<sub>1</sub>/amd) and indexed at (110) 27.31°, (101) 35.93°, (200) 39.02°, (111) 41.18°, (210) 43.98°, (211) 54.21°, and (220) 56.53°, corresponding to a tetragonal rutile structure (space group P4<sub>2</sub>/mm). The intensity ratio of the main diffraction peaks, (101) and (110) corresponding to anatase and rutile, respectively, was approximately 80:20.

Purely anatase UV 100 showed wider peaks, indicating smaller particle size as well as lower crystallinity. On the other hand, the Anatase and Rutile samples exhibited well-defined diffraction peaks confirming their highly crystalline structure.

The diffuse reflectance spectra of the anatase-containing layers (Anatase, UV 100, P25 with dominating anatase phase) and Rutile showed absorption edges below 400 nm and at 412 nm, respectively (**Fig. 3**). We plotted the spectra using the Kubelka–Munk  $F(R)$  function

$$F(R) = \frac{(1-R)^2}{2R} = \frac{\alpha}{s}, \quad (1)$$

where  $R$ ,  $\alpha$  and  $s$  are the diffuse reflectance, the absorption and scattering coefficients [26]. The optical band gap energy was determined using the following equation

$$(F(R)\text{hv})^{1/n} \sim (\text{hv}-E_g) \quad (2)$$

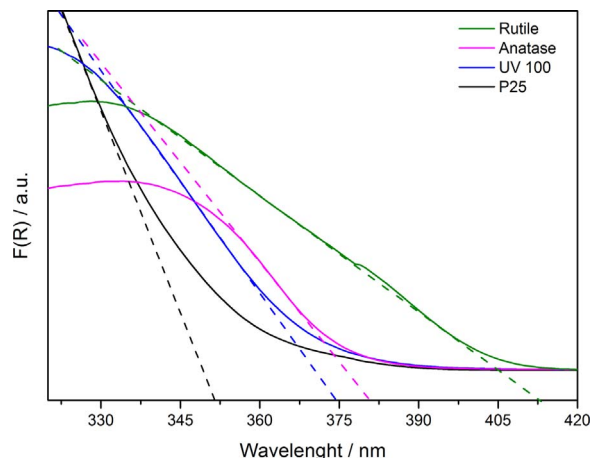


**Fig. 3.** UV-vis diffuse reflectance spectra of Rutile (olive), Anatase (magenta), UV 100 (blue) and P25 (black) layers expressed by the Kubelka–Munk function. (For interpretation of the references to colour in this figure legend, the reader is referred to the web version of this article).

where  $F(R)$ ,  $h$ ,  $\nu$ ,  $E_g$  and  $n$  are the Kubelka–Munk function, the Planck constant, the oscillation frequency, the band gap energy and the constant relating to the mode of transition. The minimal-energy state in the conduction band and the maximal-energy state in the valence band are each characterized by a  $k$ -vector in the Brillouin zone [27]. Two types of band-to-band transitions are suggested. First, direct transitions, where the  $k$ -vectors are the same and the participation of a phonon is not required to conserve momentum. Second, indirect transitions, where at least one phonon participates in the absorption or emission of a photon to conserve momentum. The constant  $n$  equals 1/2 for the allowed direct, 3/2 for the forbidden direct or 2 for the allowed indirect transitions. We checked the linearity of the plots of  $(F(R)\text{hv})^{1/n}$  against  $\text{hv}$  using  $n=2$  (allowed indirect) or  $n=1/2$  (allowed direct) to assess the mode of the transition of a given crystal. More details are provided in the review by Ohtani [28]. Using the Tauc plot, the optical band gap energies  $E_g$  for the titania layers were calculated [29]. The absorption data were fitted according to Eq. (1) for both indirect and direct allowed band gap transitions. A satisfactory fit for the allowed indirect transitions was obtained for all of the samples, giving  $E_g$  values of 3.05, 3.20, 3.20 and 3.29 eV for Rutile, Anatase, UV 100 and P25 (**Table 2**, **Fig. 4A**). As suggested by Ohtani, also a direct extrapolation of the absorption spectra, i.e.  $F(R)\text{vs}.\text{hv}$  (**Table 2**, **Fig. 4B**), was carried out giving the values of  $E_g$  of 3.05, 3.30, 3.35, 3.53 [28].

The IR characteristic group frequencies of titania were detected for all studied samples (**Fig. 5**). The main peak centered at about 400–700 cm<sup>-1</sup> is attributed to Ti–O stretching and Ti–O–Ti bridging stretching modes; the band at 960 cm<sup>-1</sup> is associated with titanyl bonds. The bands at 1640, 1190 and 1090 cm<sup>-1</sup> are due to deformation vibrations of H–O–H bonds of sorbed water while the broad bands at 1900–2300 and 3100–3600 cm<sup>-1</sup> correspond to bridging hydroxyls, which are obviously overlapped with the sorbed water [30]. Peak centered at 3670 cm<sup>-1</sup> belongs to free O–H vibrations [31].

**Table 2**

Experimental  $E_g$  values obtained for the TiO<sub>2</sub> photocatalysts using the plot of Kubelka–Munk function vs. E and the Tauc plot, respectively.

Function	Band gap/eV			
	Rutile	Anatase	UV 100	P25
$F(R)$	3.05	3.30	3.35	3.53
$(F(R) \times E)^{1/2}$	3.05	3.20	3.20	3.29

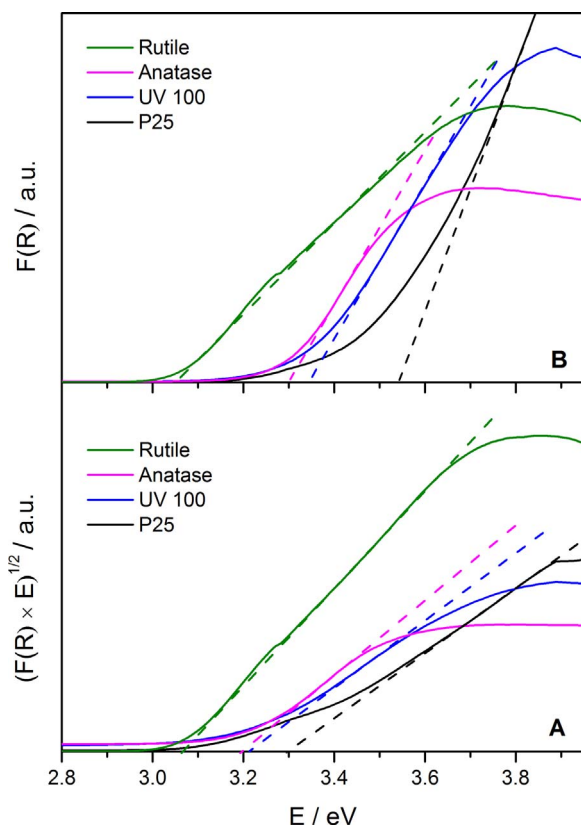


**Fig. 4.** Determination of the optical band gap ( $E_g$ ) of Rutile (olive), Anatase (magenta), UV 100 (blue) and P25 (black) layers using the Tauc plot (A) and direct plotting  $F(R)$  vs.  $E$ . Details see the text. (For interpretation of the references to colour in this figure legend, the reader is referred to the web version of this article).

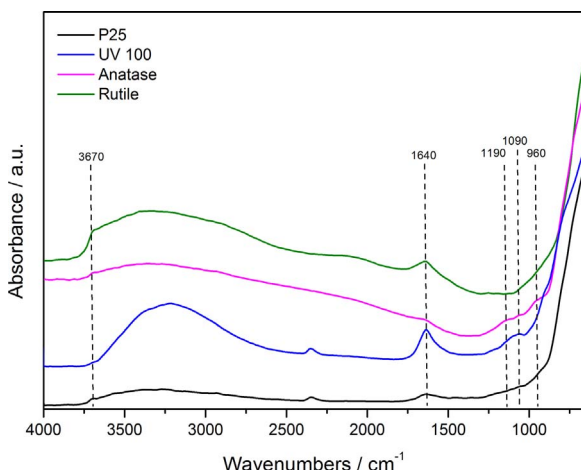


**Fig. 5.** FTIR attenuated total reflectance spectra of P25 (black), UV 100 (blue), Anatase (magenta) and Rutile (olive). (For interpretation of the references to colour in this figure legend, the reader is referred to the web version of this article).

### 3.4. Photocatalytic performance

As a test reaction, we used the photocatalytic degradation of 4-chlorophenol on titania layers because this compound is a common water pollutant that exhibits good chemical stability, undergoes negligible photolysis, and possesses relatively low adsorption on the photocatalyst surface.

First, the effect of the support on the stability of deposited layers and their photocatalytic performance was determined. Initial comparison experiments showed that the support (FTO, stainless steel, silicon)

**Table 3**

Photocatalytic performance in the degradation of 4-chlorophenol of layers of four different  $\text{TiO}_2$  powders deposited on stainless steel supports.

$\text{TiO}_2$ loading/ $\text{mg cm}^{-2}$	$k \times 10^3/\text{min}^{-1}$			
	Anatase	P25	UV 100	Rutile
0.06	1.7	1.7	1.2	0.5
0.12	1.9	3.1	1.6	0.8
0.25	3.8	5.3	2.2	1.1
0.50	6.7	7.2	2.9	1.2
1.25	13.0	10.5	4.2	1.6
2.50	15.1	12.1	4.8	1.7
0.50 mg powder	26.9	25.9	2.3	1.2

had a negligible effect on photocatalytic degradation (see SFig. 1). Therefore, stainless steel was chosen because of its advantageous properties, such as high electric conductivity, smoothness of the surface and mechanical properties. Moreover, the layers deposited on its surface exhibited very good adhesion, with no leaking of titania particles during the photocatalytic experiments and no particles were detected in the solution after the experiments. When reused, the tested layers showed no deterioration in photocatalytic performance, which is very important from the application point of view. Furthermore, the BET surface areas of the titania samples, either in powder or layer form, were practically the same, which testifies to the fact that the layers were porous with excellent accessibility to the inner surface.

Having determined the role of the support on which the titania particles were deposited we investigated their photocatalytic performance in 4-CP degradation. The results were interesting (Table 3, Fig. 6). Anatase and P25 reached the highest photocatalytic efficiency; their rate constants rose as titania mass increased. Conversely, less active were UV 100 and Rutile, both of which plateaued even at low mass ( $\sim 0.5 \text{ mg cm}^{-2}$ ). We suggest that the key parameter of photocatalytic activity was related to the structural properties (crystallinity) of the titania particles and their allotropic form.

Rutile layer, composed of particles roughly 58 nm, which corresponded to the BET surface area  $26 \text{ m}^2 \text{ g}^{-1}$  provided the crystals were approximated by spheres, displayed much lower photocatalytic activity than Anatase layer, consisting of about three-times larger particles (the BET surface area of  $10 \text{ m}^2 \text{ g}^{-1}$  corresponding to particle size of 150 nm). Anatase layers were even more active than those of P25. This result can be explained in several ways. Firstly, the direct transition of rutile facilitates the early return of excited electrons to the valence band while the indirect transition of anatase stabilizes the electrons at the lower level of its conduction band. Consequently, the extent of

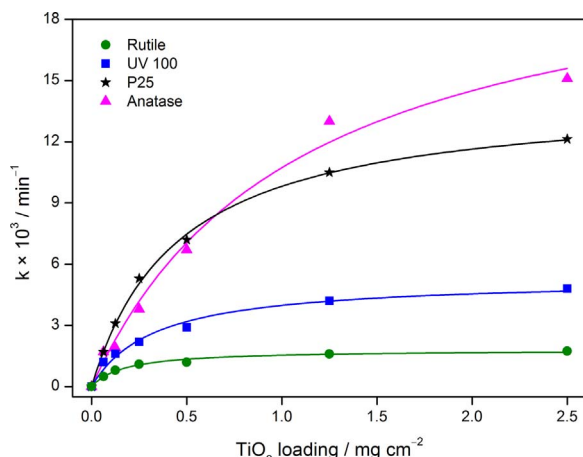


**Fig. 6.** Dependence of the first-order rate constants of 4-CP degradation on Rutile, UV 100, P25 and Anatase on mass. (For interpretation of the references to colour in this figure legend, the reader is referred to the web version of this article).

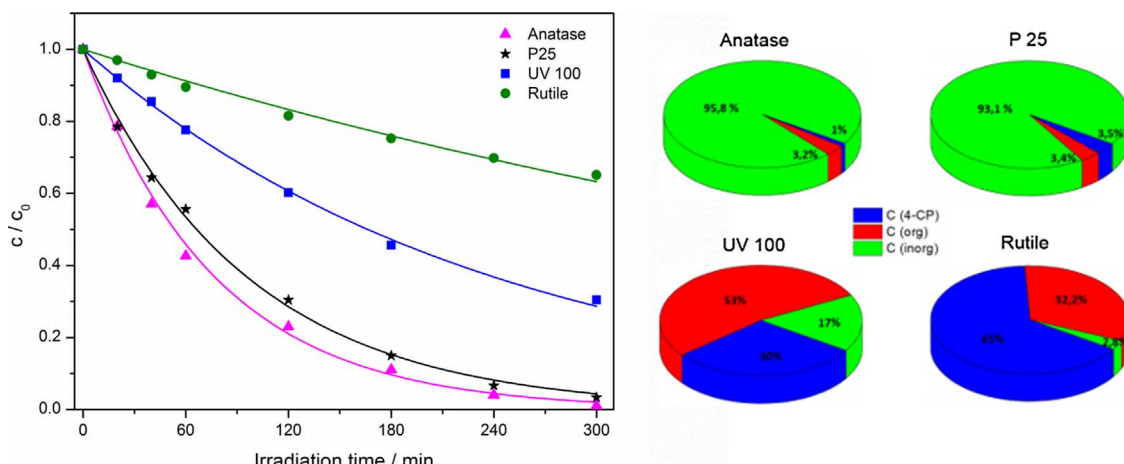


**Fig. 7.** Photocatalytic degradation of 4-chlorophenol on  $\text{TiO}_2$  layers of 5 mg deposited on stainless steel (left). Mass percentage of individual products after the irradiation time of 300 min (right).

recombination for rutile is larger than that for anatase. Secondly, the average effective mass of charge carriers is lower for anatase than for rutile, which supports faster charge carrier migration and suppresses their recombination [32]. Finally, Luttrell et al. investigated the effect of layer thickness on the charge carrier migration within anatase and rutile layers. They found that for rutile the charge carrier generated deeper in the bulk ( $> 2.5 \text{ nm}$ ) did not reach the surface and recombined while for anatase the charge carrier generation even deeper was unhindered [33]. Thus, all these observations are in agreement with the photocatalytic performance determined in this study.

Thinner P25 layers (the BET surface area of  $57 \text{ m}^2 \text{ g}^{-1}$  corresponding to particle size of 26 nm) exhibited a comparable photocatalytic activity to corresponding Anatase layers, while for thicker layers Anatase was more active. Nevertheless, the photocatalytic activity of P25 was high which agrees with the generally observed outstanding performance of this photocatalyst. The superiority of Anatase at high loading is probably due to its very high crystallinity and its well-developed crystals practically without defects.

UV 100, consisting of very small anatase particles with the largest surface area (the BET surface area of  $271 \text{ m}^2 \text{ g}^{-1}$  corresponding to particle size of 5.5 nm), was the least active [34]. One reason for this might be that its less well-developed crystals contain a substantial concentration of defects that function as recombination centers. Another reason might the presence of an amorphous phase within the UV 100 crystals.

Besides the role of crystallinity and the presence of defects, the difference in photocatalytic activity of large and small particles of anatase can be generally explained by taking into account kinetic differences in the primary photoprocesses of photogenerated charge carriers in the semiconductor particles of different sizes. The internal recombination of electron with positive hole, on one hand, and the transfers of these charge carriers through interface to their corresponding reactants, on the other hand, are parallel processes; the kinetic competition between these two processes determines the actual photocatalytic activity. From the kinetic point of view, recombination can be considered as a second-order process because its rate is directly proportional to the product of concentrations of electrons and holes in the particle. On the contrary, interfacial transfers of charge carriers are first order processes because their rates depend only on the concentration of the particular charge carrier multiplied by the concentration of the corresponding redox reactants on the particle surface. Assuming a generally low intensity of continuous irradiation, under which two-photon processes can be practically neglected (unlike laser flash photolysis), only one electron-hole pair is formed at certain time in a single semiconductor particle. Due to extremely high reactivity and correspondingly short lifetimes of the separated charges, they finish

their reactions, on statistical average, a long time before the next photon is absorbed in the same particle and another electron-hole pair is photogenerated. The primary photoprocesses take place in the semiconductor phase; thus, their reaction volume is limited to the geometrical volumes of the particles. Supposing the occurrence of only single electron/hole pair in a particle, the actual concentrations of charge carriers will decrease with increasing particle size. The decreased concentration of charge carriers in larger particles will slow the primary photoprocesses (i.e., the recombination and interfacial transfers of charge carriers); however, the rate of internal recombination, as a second order reaction, will decrease more progressively than the corresponding rates of charge transfer behaving like pseudo-first order reactions. As the total rate of a photocatalytic degradation reaction is determined by their ratio, it should increase with increasing particle size, which is in agreement with our observation.

#### 3.4.1. Mineralization of 4-CP

Besides the rate constants, also the degree of 4-chlorophenol mineralization is of fundamental importance for a deeper understanding and relevant comparison of the photocatalytic performance of individual  $\text{TiO}_2$  layers [35,36]. Regarding the application of photocatalysis in the purification of water, a high degree of mineralization is required because of the potential risk due to presence of aromatic or nonaromatic organic products, formed in the course of step-by-step pollutant degradation.

The most photocatalytically active Anatase and P25 exhibited a very high degree of mineralization reaching almost 100 per cent (Fig. 7). This implies that vast majority of organic carbon was converted into carbon dioxide, while only a small part of about 3 per cent remained in the solution as organic carbon. On the other hand, for the UV 100 and Rutile layers, the percentage of inorganic carbon was less than 20 per cent and the rest remained in the form of 4-CP or other organic compounds.

#### 3.4.2. Titania layers vs. powders

A comparison of the photocatalytic performance of the powders and corresponding layers deposited on the steel support showed that for the two most active samples (Anatase and P25) the powders were more efficient (Fig. 8). However, in the case of the much slower photocatalytic reaction for the less active photocatalysts (UV 100 and Rutile), this effect was practically negligible.

This observation is not surprising because, due to a very fast photocatalytic reaction on the surface or in the immediate environment of the photocatalyst, transport phenomena play an important role. In the case of the porous layers on the solid support, the slowing of the transport of 4-CP molecules is to be expected compared with separate

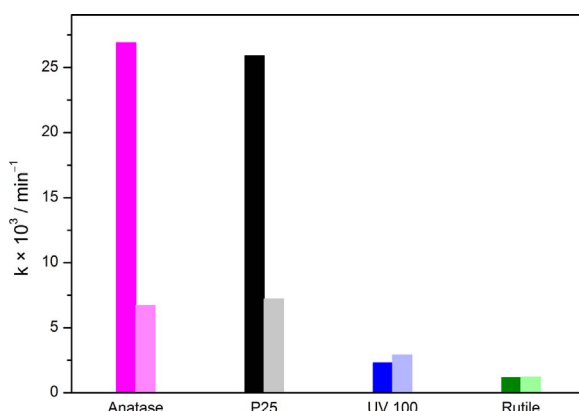


Fig. 8. Comparison between the first-order rate constants of 4-CP degradation on  $\text{TiO}_2$  (2 mg) in the form of a powder (dark shade) and a layer on stainless steel (light shade).

particles homogeneously dispersed within the whole volume of the reactor. Furthermore, the absorption of UV light within the layers was predominant close to the outer surface but limited deeper in the layer near the support. With the powders homogeneously dispersed within the solution, such a limitation is absent.

However, even with layers, the rate of photocatalytic degradation was sufficient for the efficient removal of the pollutant and, due to the ease of layer application without the difficult separation of very fine particles, their use in the remediation of polluted water can be recommended.

#### 3.4.3. Mechanism of 4-CP degradation process

The modeling by density functional theory (DFT) of the degradation of 4-chlorophenol molecules by OH radicals showed that the hydroxylation of the aromatic ring and its opening can occur in parallel releasing hydroperoxyl radical and hydroxyl radical, respectively [37,38]. The restored OH radical can either further oxidize the primary ring opening product or attack another molecule of 4-chlorophenol. These computational results are in good agreement with the photocatalytic degradation observations made using both  $\text{ZnO}$  and  $\text{TiO}_2$  photocatalysts [37,38].

Specifically, the first branch of the mechanism starts with a preferential abstraction of the hydrogen atom at the position 7 (Fig. 9), leading to a molecule of water and 4-chlorophenoxy radical. Comparing energy characteristics, this reaction is the most favorable from all possible OH attacks onto 4-chlorophenol molecule. Afterwards, chlorine is abstracted and hydrochloric acid is formed. The final products of this branch are the experimentally identified aromatic products hydroquinone and benzoquinone.

In the parallel branch, the addition of OH radical into all non-substituted 2, 3, 5, and 6 positions runs extremely fast. Also the subsequent abstractions of hydrogen atoms from the same positions by molecular triplet oxygen are strongly exothermic and proceed very fast. After a number of intermediates, ring, ring-opening compounds are formed as

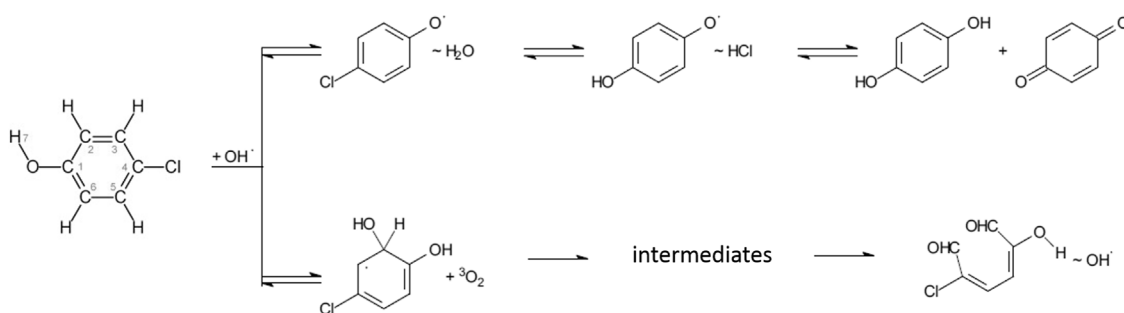


Fig. 9. Simplified scheme of the photocatalytic 4-chlorophenol degradation.

products under restoration of OH radical.

Due to a high reactivity and short lifetime of OH radicals in water, a direct detection is very difficult. For the indirect detection of OH radicals, we employed a fluorescence spectroscopy using coumarin derivatives [39]. For the detection of OH radicals, we employed an aqueous  $10^{-4}$  M solution of coumarin-3-carboxylic acid. This acid reacted with OH radicals to produce 7-OH-coumarin-3-carboxylic acid, which was excited at 365 nm and emitted a strong fluorescence at 442 nm. OH radicals were formed by irradiating of  $\text{TiO}_2$  nanoparticle layers with 365 nm light. SFig. 2 shows the intensive fluorescence of 7-OH-coumarin-3-carboxylic acid that confirmed the formation of OH radicals on the P25 layer of  $0.1 \text{ mg cm}^{-2}$ . The formation of 7-OH-coumarin-3-carboxylic acid after 30 s of irradiation is shown in SFig. 3.

The 4-chlorophenol degradation pathway is complex, leading to the formation of 4-chlorocatechol, hydroquinone, and nonaromatic organic compounds, as the primary intermediates [40]. Our previous studies have shown that the concentration of aromatic intermediates was close to the detection limit and often could not be reasonably evaluated [37,38,41].

The photocatalytic process itself involves two different mechanisms: a direct transfer of charge carriers and an attack of radicals; depending on the reaction conditions, these mechanisms may act separately or jointly. The radicals can be formed by the reaction of photo-generated holes with surface hydroxyl groups or with sorbed water. According to Yu et al., this reactions contribute to an enhancement of photocatalytic activity because the recombination of electron-hole pairs would be suppressed [42].

Nevertheless, when a radical scavenger is used, only the direct charge transfer controls the mechanism of pollutant degradation. To assess the role of a radical scavenger present in wastewaters that is to be photocatalytically purified, we performed additional experiments. We added 2-propanol, a radical scavenger; in a thousand-fold excess either at the very beginning or during the reaction course. Such a high concentration would practically stop the 4-chlorophenol degradation if only the radical is responsible.

The addition of 2-propanol during the reaction drastically slowed the rate of 4-chlorophenol photocatalytic degradation for all of the tested samples (Fig. 10). However, there were significant differences in reaction deceleration; in particular, slowing was far more pronounced for the most active sample, Anatase (376 times), than for the least active, Rutile (7 times) (Table 4).

Moreover, interestingly, when 2-propanol was added at the reaction start we obtained similar results (Fig. 11). Anatase had the lowest rate constant ( $33 \times 10^{-5} \text{ min}^{-1}$ ), while Rutile exhibited the highest photocatalytic activity ( $90 \times 10^{-5} \text{ min}^{-1}$ ).

Therefore, it seems that for Rutile the direct transfer mechanism was dominant and that the formation of radicals on its surface was rather restricted. Conversely, for Anatase, the mechanism was mostly controlled by the radicals, with the effect of direct transfer being almost negligible.

A comparison of the rate constant of Anatase and UV 100 layers showed something quite remarkable. The reaction rate for UV 100

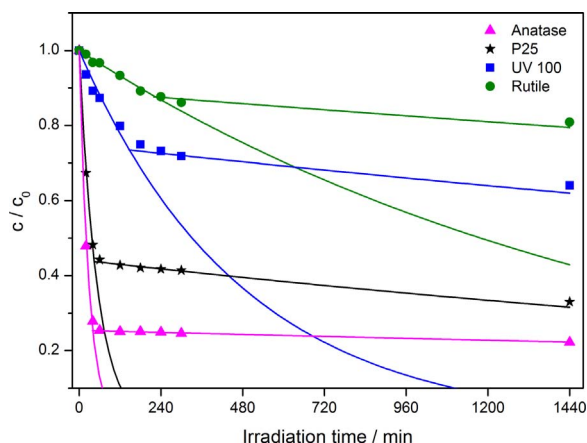


**Fig. 10.** Effect of OH radical scavenger (2-propanol) added in different time course of photocatalytic degradation of 4-CP on titania powder of 2 mg.

**Table 4**

The effect of a radical scavenger (2-propanol) on the 1st order rate constant of photocatalytic degradation of 4-CP on various titania powders (2 mg) if added at the beginning ( $k^*$ ) and during the reaction ( $k^{**}$ ). The rate constant  $k$  refers to the absence of the scavenger.

Sample	$k^* \times 10^5/\text{min}^{-1}$	$k \times 10^5/\text{min}^{-1}$	$k^{**} \times 10^5/\text{min}^{-1}$	$k/k^{**}$
Anatase	33	3400	9	376
P25	84	1900	23	83
UV 100	72	210	13	16
Rutile	90	59	8	7

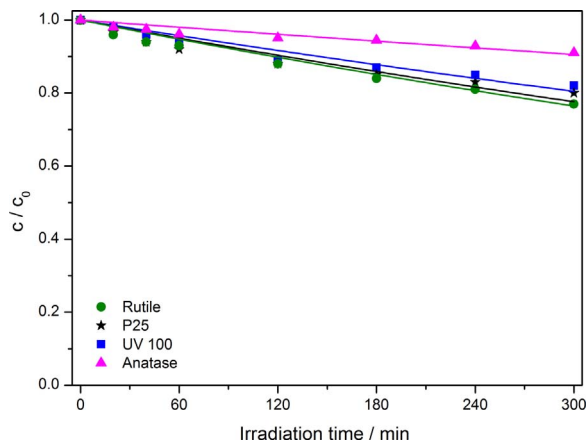


**Fig. 11.** Effect of OH radical scavenger (2-propanol) added at the beginning of the photocatalytic degradation of 4-CP on titania powder of 2 mg.

( $72 \times 10^{-5} \text{ min}^{-1}$ ) was two-times higher than that for Anatase ( $33 \times 10^{-5} \text{ min}^{-1}$ ), even though they are both purely anatase samples. We suggest that this is related to the higher adsorption of 4-CP on the large, less crystalline and defective surface of UV 100.

The photocatalytic performance of P25 in the presence of the scavenger lay somewhere between that of anatase and rutile, but with a predominance of the direct charge transfer of the rutile phase, which is consistent with the different roles direct charge transfer plays for these two photocatalysts. Moreover, this P25 performance was further enhanced by the sorption of 4-CP, which was three-times higher for P25 than for Anatase (Fig. 12). This indicates that the sorption of the 4-CP molecules on the titania surface played an important role when the radical mechanism was suppressed (Fig. 11).

This study showed that the photocatalytic performance of layers prepared by electrophoretic deposition depended substantially on the structural and morphologic properties of titania particles, especially on

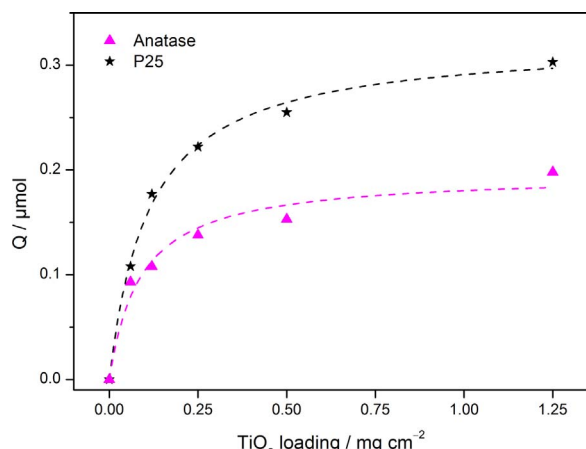


**Fig. 12.** Sorption of 4-chlorophenol on Anatase and P25 powders.

their allotropic form (anatase vs. rutile), crystallinity, presence of defects and their particle size. For well-developed anatase crystals, a high rate of the degradation of 4-chlorophenol and its almost complete mineralization was achieved. Furthermore, we found that the mechanism of the 4-chlorophenol photocatalytic degradation on anatase was controlled by the formation of radicals, while on rutile the direct charge transfer was dominant.

#### 4. Conclusions

We developed an electrophoretic deposition method that enables to quantitatively deposit a broad range of powders on conductive substrates without using additives, which ensured an effective use of material without any losses and removed the necessity to determine the mass of the deposited particles. As the layers exhibit good adhesion to the substrate and high stability in aqueous media, they are suitable as photocatalysts for environmental applications. Moreover, as no treatment at increased temperature is required, this method is suitable for heat-sensitive materials and substrates.

Based on the obtained correlation between the structural and morphologic properties of deposited powders (especially allotropic form, crystallinity and particle size), the most suitable materials for the efficient degradation of pollutants can be selected. For the well-developed anatase crystals, a high rate of the degradation of 4-chlorophenol and its almost complete mineralization were achieved. This feature, which is often overlooked in photocatalytic studies, is of fundamental importance regarding the application of photocatalysis in the purification of water. Such a high degree of mineralization is required due to the potential risk of aromatic or nonaromatic organic products.

The mechanistic study has shown that the structural properties of photocatalyst and the presence of potential radical scavenger decisively influence the mechanism itself of the pollutant degradation. Therefore, when selecting the most suitable photocatalytical system, this aspect should be taken into account.

To sum-up, the optimum selection of the photocatalytic technology for the specific environmental application is rather complex and requires a detailed knowledge about all the relevant aspects.

Our preceding research showed that the photocatalytic activity of titania layers prepared by doctor-blading can be increased by doping with carbon nanostructures [41,43]. Therefore, as a further step, we have started a study into the possibility of the preparation of doped titania layers by EPD. Preliminary experiments with single layer graphene oxide sheets have shown that this technique is very suitable for the deposition of such doped layers.

## Acknowledgments

The authors are grateful to the Czech Science Foundation (GACR) for financial support (Grant No. 17–18972S). This work was supported by the Ministry of Education, Youth and Sports of the Czech Republic and The European Union – European Structural and Investments Funds in the frame of Operational Programme Research, Development and Education – project Pro-NanoEnviCz (Project No.CZ.02.1.01/0.0/0.0/16\_013/0001821). Project Pro-NanoEnviCz provided an excess to the Micromeritics 3Flex apparatus. The authors thank J. Jirkovsky (J. Heyrovsky Institute of Physical Chemistry, Prague) for the valuable suggestions for the explanation of the reaction mechanisms.

## Appendix A. Supplementary data

Supplementary data associated with this article can be found, in the online version, at <https://doi.org/10.1016/j.apcatb.2018.01.035>.

## References

- [1] C. Liu, C.P. Huang, C. Hu, Y. Juang, C. Huang, Photoelectrochemical degradation of dye wastewater on TiO<sub>2</sub>-coated titanium electrode prepared by electrophoretic deposition, *Sep. Purif. Technol.* 165 (2016) 145–153, <http://dx.doi.org/10.1016/j.seppur.2016.03.045>.
- [2] W. Lin, C. Chen, H. Tang, Y. Hsiao, J. Ruhsing, C. Hu, C. Huang, Electrochemical photocatalytic degradation of dye solution with a TiO<sub>2</sub>-coated stainless steel electrode prepared by electrophoretic deposition, *Appl. Catal. B: Environ.* 141 (2013) 32–41.
- [3] V. Pifferi, F. Spadavecchia, G. Cappelletti, E.A. Paoli, C.L. Bianchi, L. Falciai, Electrodeposited nano-titania films for photocatalytic Cr (VI) reduction, *Catal. Today* 209 (2013) 8–12, <http://dx.doi.org/10.1016/j.cattod.2012.08.031>.
- [4] E. Pramauro, M. Vincenti, V. Augugliaro, L. Palmisano, Photocatalytic degradation of monuron in aqueous TiO<sub>2</sub> dispersions, *Environ. Sci. Technol.* 27 (1993) 1790–1795, <http://dx.doi.org/10.1021/es00046a005>.
- [5] A. Scalfani, L. Palmisano, M. Schiavello, Influence of the preparation methods of titanium dioxide on the photocatalytic degradation of phenol in aqueous dispersion, *J. Phys. Chem.* 94 (1990) 829–832, <http://dx.doi.org/10.1021/j100365a058>.
- [6] R.R. Bacsa, J. Kiwi, Effect of rutile phase on the photocatalytic properties of nanocrystalline titania during the degradation of p-coumaric acid, *Appl. Catal. B Environ.* 16 (1998) 19–29, [http://dx.doi.org/10.1016/S0926-3373\(97\)00058-1](http://dx.doi.org/10.1016/S0926-3373(97)00058-1).
- [7] J. Low, B. Cheng, J. Yu, Surface modification and enhanced photocatalytic CO<sub>2</sub> reduction performance of TiO<sub>2</sub>: a review, *Appl. Surf. Sci.* 392 (2017) 658–686, <http://dx.doi.org/10.1016/j.apsusc.2016.09.093>.
- [8] D. He, Y. Li, I. Wang, J. Wu, Y. Yang, Q. An, Carbon wrapped and doped TiO<sub>2</sub> mesoporous nanostructure with efficient visible-light photocatalysis for NO removal, *Appl. Surf. Sci.* 391 (2017) 318–325, <http://dx.doi.org/10.1016/j.apsusc.2016.06.186>.
- [9] C.S. Lugo-Vega, B. Serrano-Rosales, H. de Lasa, Immobilized particle coating for optimum photon and TiO<sub>2</sub> utilization in scaled air treatment photo reactors, *Appl. Catal. B Environ.* 198 (2016) 211–223, <http://dx.doi.org/10.1016/j.apcatb.2016.05.063>.
- [10] E. Bailón-García, A. Elmouahidi, M.A. Álvarez, F. Carrasco-Marín, A.F. Pérez-Cadenas, F.J. Maldonado-Hódar, New carbon xerogel-TiO<sub>2</sub> composites with high performance as visible-light photocatalysts for dye mineralization, *Appl. Catal. B Environ.* 201 (2017) 29–40, <http://dx.doi.org/10.1016/j.apcatb.2016.08.015>.
- [11] R. Zouzelka, J. Rathousky, Photocatalytic abatement of NO<sub>x</sub> pollutants in the air using commercial functional coating with porous morphology, *Appl. Catal. B Environ.* 217 (2017) 466–476, <http://dx.doi.org/10.1016/j.apcatb.2017.06.009>.
- [12] H.G. Krueger, A. Knote, U. Schindler, H. Kern, A.R. Boccaccini, Composite ceramic metal coatings by means of combined electrophoretic deposition, *J. Mater. Sci.* 39 (2004) 839–844.
- [13] C. Chen, S. Chen, D. Liu, Electrophoretic deposition forming of porous alumina membranes, *Acta Mater.* 47 (1999) 2717–2726, [http://dx.doi.org/10.1016/S1359-6454\(99\)00140-8](http://dx.doi.org/10.1016/S1359-6454(99)00140-8).
- [14] B. Ferrari, R. Moreno, The conductivity of aqueous Al<sub>2</sub>O<sub>3</sub> slips for electrophoretic deposition, *Mater. Lett.* 28 (1996) 353–355, [http://dx.doi.org/10.1016/0167-577X\(96\)00075-4](http://dx.doi.org/10.1016/0167-577X(96)00075-4).
- [15] B. Ferrari, R. Moreno, Electrophoretic deposition of aqueous alumina slips, *J. Eur. Ceram. Soc.* 17 (1997) 549–556, [http://dx.doi.org/10.1016/S0955-2219\(96\)00113-6](http://dx.doi.org/10.1016/S0955-2219(96)00113-6).
- [16] N. Heavens, Electrophoretic deposition as a processing route for ceramics, in: G.P. Binner (Ed.), *Adv. Ceram. Process.*, 1st ed., 1990, pp. 255–283 Park Ridge (NJ).
- [17] N. Sato, M. Kawachi, K. Noto, N. Yoshimoto, M. Yoshizawa, Effect of particle size reduction on crack formation in electrophoretically deposited YBCO films, *Phys. C Supercond.* 357–360 (2001) 1019–1022, [http://dx.doi.org/10.1016/S0921-4534\(01\)00510-X](http://dx.doi.org/10.1016/S0921-4534(01)00510-X).
- [18] L. Besra, M. Liu, A review on fundamentals and applications of electrophoretic deposition (EPD), *Prog. Mater. Sci.* 52 (2007) 1–61, <http://dx.doi.org/10.1016/j.pmatsci.2006.07.001>.
- [19] R. Powers, Electrophoretic forming of Beta-Alumina ceramic, *J. Electrochem. Soc.* 122 (1975) 482–486, <http://dx.doi.org/10.1149/1.2134246>.
- [20] M. Kawakita, T. Uchikoshi, J. Kawakita, Y. Sakka, Preparation of crystalline-oriented titania photoelectrodes on ITO glasses from a 2-propanol-2,4-pentanediol solvent by electrophoretic deposition in a strong magnetic field, *J. Am. Ceram. Soc.* 92 (2009) 984–989, <http://dx.doi.org/10.1111/j.1551-2916.2009.02947.x>.
- [21] M. Basu, R.N. Randall, C.A. Mayo, Fabrication of dense zirconia electrolyte films for tubular solid oxide fuel cells by electrophoretic deposition, *J. Am. Ceram. Soc.* 84 (2001) 33–40.
- [22] W. Vandeperre, L. VanDerBiest, O. Clegg, Silicon carbide laminates with carbon interlayers by electrophoretic deposition, in: A. Fuentes, M. Martinez-Esnaola, J.M. Daniel (Eds.), C. 96—Proc. FIRST Int. Conf. Ceram. Met. MATRIX Compos. PTS 1 2 (1997) 567–573.
- [23] S. Radice, C.R. Bradbury, J. Michler, S. Mischler, Critical particle concentration in electrophoretic deposition, *J. Eur. Ceram. Soc.* 30 (2010) 1079–1088, <http://dx.doi.org/10.1016/j.jeurceramsoc.2009.08.021>.
- [24] B. Ohtani, D. Li, R. Abe, What is Degussa (Evonik) P25? Crystalline composition analysis, reconstruction from isolated pure particles and photocatalytic activity test, *J. Photochem. Photobiol. A: Chem.* 216 (2010) 179–182, <http://dx.doi.org/10.1016/j.jphotochem.2010.07.024>.
- [25] J. Rathouský, V. Kalousek, M. Kolář, J. Jirkovský, Mesoporous films of TiO<sub>2</sub>(2) as efficient photocatalysts for the purification of water, *Photochem. Photobiol. Sci.* 10 (2011) 419–424, <http://dx.doi.org/10.1039/c0pp00185f>.
- [26] P. Kubelka, New contributions to the optics of intensely light-scattering materials. Part I, *J. Opt. Soc. Am.* 38 (1948) 448–457, <http://dx.doi.org/10.1364/JOSA.38.000448>.
- [27] N. Serpone, E. Pelizzetti, Optical absorption of colloidal semiconductors particles: Mie theory, *Photocatal. Fundam. Appl.*, John Wiley & Sons, 1989, pp. 1–650.
- [28] B. Ohtani, Photocatalysis A to Z—What we know and what we do not know in a scientific sense, *J. Photochem. Photobiol. C Photochem. Rev.* 11 (2010) 157–178, <http://dx.doi.org/10.1016/j.jphotochemrev.2011.02.001>.
- [29] J. TAUC, Optical Properties and electronic structure of amorphous, *Mater. Res. Bull.* 3 (1968), [http://dx.doi.org/10.1016/0025-5408\(68\)90023-8](http://dx.doi.org/10.1016/0025-5408(68)90023-8).
- [30] L. Li, J. Yan, T. Wang, Z.-J. Zhao, J. Zhang, J. Gong, N. Guan, Sub-10 nm rutile titanium dioxide nanoparticles for efficient visible-light-driven photocatalytic hydrogen production, *Nat. Commun.* 6 (2015) 5881, <http://dx.doi.org/10.1038/ncomms6881>.
- [31] C. Arrouvel, M. Digne, M. Breysse, H. Toulhoat, P. Raybaud, Effects of morphology on surface hydroxyl concentration: a DFT comparison of anatase-TiO<sub>2</sub> and γ-alumina catalytic supports, *J. Catal.* 222 (2004) 152–166, <http://dx.doi.org/10.1016/j.jcat.2003.10.016>.
- [32] J. Zhang, P. Zhou, J. Liu, J. Yu, New understanding of the difference of photocatalytic activity among anatase, rutile and brookite TiO<sub>2</sub>, *Phys. Chem. Chem. Phys.* 16 (2014) 20382–20386, <http://dx.doi.org/10.1039/C4CP02210G>.
- [33] T. Luttrell, S. Halpegamage, J. Tao, A. Kramer, E. Sutter, M. Batzill, Why is anatase a better photocatalyst than rutile?—Model studies on epitaxial TiO<sub>2</sub> films, *Sci. Rep.* 4 (2015) 4043, <http://dx.doi.org/10.1038/srep04043>.
- [34] J. Zita, J. Krysa, U. Černigoj, U. Lavrenčič-Štangar, J. Jirkovský, J. Rathouský, Photocatalytic properties of different TiO<sub>2</sub> thin films of various porosity and titania loading, *Catal. Today* 161 (2011) 29–34, <http://dx.doi.org/10.1016/j.cattod.2010.11.084>.
- [35] A. Mills, J. Wang, Photomineralisation of 4-chlorophenol sensitised by TiO<sub>2</sub> thin films, *J. Photochem. Photobiol. A Chem.* 118 (1998) 53–63, [http://dx.doi.org/10.1016/S1010-6030\(98\)00361-X](http://dx.doi.org/10.1016/S1010-6030(98)00361-X).
- [36] J. Theurich, M. Lindner, D.W. Bahnemann, Photocatalytic degradation of 4-chlorophenol in aerated aqueous titanium dioxide suspensions: a kinetic and mechanistic study, *Langmuir* 12 (1996) 6368–6376, <http://dx.doi.org/10.1021/la960228t>.
- [37] V.-M. Guérin, R. Zouzelka, H. Bibova-Lipsova, J. Jirkovský, J. Rathouský, T. Pauporté, Experimental and DFT study of the degradation of 4-chlorophenol on hierarchical micro-/nanostructured oxide films, *Appl. Catal. B Environ.* 168–169 (2015) 132–140, <http://dx.doi.org/10.1016/j.apcatb.2014.12.041>.
- [38] J. Hynek, V. Kalousek, R. Zouzelka, P. Bezdička, P. Dzik, J. Rathouský, J. Demel, K. Lang, High photocatalytic activity of transparent films composed of ZnO nanosheets, *Langmuir* 30 (2014) 380–386, <http://dx.doi.org/10.1021/la404017q>.
- [39] Y. Nosaka, M. Nishikawa, A.Y. Nosaka, Spectroscopic investigation of the mechanism of photocatalysis, *Molecules* 19 (2014) 18248–18267, <http://dx.doi.org/10.3390/molecules19118248>.
- [40] X. Li, J.W. Cubbage, T.A. Tetzlaff, W.S. Jenks, Photocatalytic degradation of 4-chlorophenol. 1. The hydroquinone pathway, *J. Org. Chem.* 64 (1999) 8509–8524, <http://dx.doi.org/10.1021/jo990820y>.
- [41] R. Zouzelka, Y. Kusumawati, M. Remzova, J. Rathouský, T. Pauporté, Photocatalytic activity of porous multiwalled carbon nanotube-TiO<sub>2</sub> composite layers for pollutant degradation, *J. Hazard. Mater.* 317 (2016) 52–59, <http://dx.doi.org/10.1016/j.hazmat.2016.05.056>.
- [42] J. Yu, G. Wang, B. Cheng, M. Zhou, Effects of hydrothermal temperature and time on the photocatalytic activity and microstructures of bimodal mesoporous TiO<sub>2</sub> powders, *Appl. Catal. B Environ.* 69 (2007) 171–180, <http://dx.doi.org/10.1016/j.apcatb.2006.06.022>.
- [43] Y. Kusumawati, T. Pauporté, B. Viana, R. Zouzelka, M. Remzova, J. Rathouský, Mesoporous TiO<sub>2</sub>/graphene composite films for the photocatalytic degradation of eco-persistent pollutants, *SPIE Proc.* 10105 (2017) 1–10, <http://dx.doi.org/10.1117/12.2253132>.